

# Angle-Resolved Attosecond Streaking of Twisted Attosecond Pulses

Irfana N. Ansari,<sup>1</sup> Deependra S. Jadoun,<sup>1</sup> and Gopal Dixit<sup>1,\*</sup>

<sup>1</sup>*Department of Physics, Indian Institute of Technology Bombay, Powai, Mumbai 400076, India*

(Dated: June 3, 2020)

The present work focuses on the characterisation of the amount of orbital angular momentum (OAM) encoded in the twisted attosecond pulses via energy- and angle-resolved attosecond streaking in pump-probe setup. It is found that the photoelectron spectra generated by the linearly polarised twisted pulse with different OAM values exhibit angular modulations, whereas circularly polarised twisted pulse yields angular isotropic spectra. It is demonstrated that the energy- and angle-resolved streaking spectra are sensitive to the OAM values of the twisted pulse. Moreover, the different combinations of the polarisation of the twisted pump pulse and strong infrared probe pulse influence the streaking spectra differently. The characterisation of the OAM carrying twisted attosecond pulses opens up the possibility to explore helical light-matter interaction on attosecond timescale.

PACS numbers:

Complete characterisation of attosecond pulses is essential to harness the full potential of such pulses in capturing ultrafast electron processes and extracting meaningful interpretations of time-resolved measurements [1, 2]. Different techniques are in practice to characterise the temporal structure of the attosecond pulses such as attosecond streaking and RABBITT [3–5]. Both these methods yield information about pulse duration, carrier energy, and chirp of the attosecond pulses [6, 7]. Recently, attosecond streaking method has been extended to characterise the carrier-envelope phase [8] and extract the polarisation state [9] of the isolated attosecond pulse. In this work, energy- and angle-resolved attosecond streaking (AAS) method is employed to characterise the orbital angular momentum (OAM) of twisted attosecond pulses.

The polarisation property of light is associated with its spin angular momentum, whereas the spatial profile of the wave front is connected to the OAM of the light [10]. Light with non-zero OAM is known as twisted light and Laguerre-Gaussian light beam is an example of such light and considered in this work. OAM of the light has found numerous applications in various fields since its first realisation [11–19]. These applications have motivated scientists to generate ultrashort twisted pulses in the extreme ultraviolet (XUV) energy regime to probe attosecond electron motion. In recent years, series of works have been carried out to up-convert OAM carrying infrared (IR) beam to the XUV beam using high harmonic generation (HHG) [20–28]. A non-collinear method has been applied to generate linearly polarised twisted light with relatively low OAM via HHG [29–31]. These state-of-the-art HHG experiments provided an avenue for the generation of coherent attosecond XUV pulses with desirable OAM properties. However, no claim of generating such pulses can be made without measurement of the OAM encoded in the twisted XUV pulses with no *a priori* assumptions. This is an uncharted territory and main

focus of the present work.

In this work, the concept of the standard attosecond streak camera is extended in three-dimensions as the twisted XUV pulse has a complex spatial structure. The energy- and angle-resolved photoelectron spectra are simulated as a function of pump-probe delay time for different polarisations of the twisted XUV pump pulse and IR probe pulse. The pump pulse induces a single-photon ionisation and liberated photoelectron is streaked by the synchronized IR pulse having the plane wavefront and zero OAM. Kaneyasu *et al.* have performed the photoionisation of helium by the twisted XUV beam at synchrotron and discussed the possibility of observing the violation of the standard electric dipole selection rules [32]. Boning *et al.* have discussed the streaking of twisted x-waves within dipole approximation with relatively weak continuous IR beam [33]. The influences of the projection of the total angular momentum, the opening angle and the impact parameter on the streaking spectra have been discussed [33]. Recently, the formalism of two-photon ionisation and its consequences in photoionisation time delay have been discussed [34].

The transition amplitude, within strong-field approximation, from a ground state to a continuum state  $|k\rangle$  with momentum  $\mathbf{k}$  is expressed as

$$a_{\mathbf{k}}(\tau) = -i \int_{-\infty}^{+\infty} dt e^{i[I_p t - \Phi(\mathbf{k}, t)]} \mathbf{E}_X(t - \tau) \mathbf{d}_{\mathbf{p}(t)}, \quad (1)$$

where  $I_p$  is the ionisation potential of the atom,  $\Phi(\mathbf{k}, t) = \int_t^{+\infty} dt' \mathbf{p}^2(t')/2$  is Volkov phase with  $\mathbf{p}(t) = \mathbf{k} + \mathbf{A}(t)$  as the instantaneous momentum of the photoelectron in IR field,  $\mathbf{A}(t)$  being the vector potential such that  $\mathbf{E}(t) = -\partial \mathbf{A}(t)/\partial t$ .  $\mathbf{E}_X(t) = \tilde{\mathbf{E}}_X(t) \exp[-i\Omega t]$  is the XUV field with  $\tilde{\mathbf{E}}_X(t)$  as the envelope and  $\Omega$  as the central energy of the XUV field. The parameter  $\tau$  is the time delay between the two pulses, and  $\mathbf{d}_{\mathbf{p}(t)}$  is the transition amplitude from the ground state to the continuum state  $|\mathbf{p}(t)\rangle$  with kinetic momentum  $\mathbf{p}(t)$ . In the presence of

an IR field, the phase accumulated by the photoelectron, during its motion in the continuum from  $t$  to  $+\infty$ , is  $\delta\Phi(t) = \Phi(\mathbf{k}, t) - I_p t$ . Note that strong-field approximation is appropriate as  $\omega \ll I_p$  with  $\omega$  as the frequency of the IR field, which only interacts with the emitted photoelectron.

Twisted XUV pulse induced photoionisation and exchange of the OAM larger than one unit in photoionisation has been manifested. As a result, the standard dipole selection rules get modified [35, 36]. The modified selection rules for electronic transitions read as  $|l_f - l_i| \leq |l| + 1$ ,  $m_f - m_i = l \pm 1$  and  $l_f - l_i + |l| + 1$  is even. Here,  $l_f(m_f)$  and  $l_i(m_i)$  are the final and the initial orbital angular (magnetic) quantum numbers of electronic states, respectively; and  $l$  is the topological charge of the twisted XUV pulse. It is evident from the selection rules that only two values of  $l_f = l \pm 1$  are allowed when the twisted XUV pulse with  $l \geq 0$  ionises hydrogen atom ( $l_i = 0$ ). In such situation, photoionisation transition amplitude reads as

$$\mathbf{d}_k = \frac{i\Omega\sqrt{2l}}{2\pi w_0^{l+1}} \left[ \frac{C_1 i^{l+1}}{(-1)^{l+1}} d_k^{l+1} Y_{l+1}^{l+1}(\theta_k, \phi_k) + \frac{C_2}{(-1)^l} \left\{ a i^{l-1} d_k^{l-1} Y_{l-1}^{l-1}(\theta_k, \phi_k) + b i^{l+1} d_k^{l+1} Y_{l+1}^{l-1}(\theta_k, \phi_k) \right\} \right]. \quad (2)$$

Here,  $w_0$  is the beam waist; and  $C_1 = 2^l(l+1)! [4\pi/(2l+3)!]^{1/2}$ ,  $C_2 = 2^{l+1} l! \pi [2/3(2l+1)!]^{1/2}$ ,  $a = [3(2l+1)/4\pi(2l-1)]^{1/2} C_{l,1,0,0}^{l-1,0} C_{l,1,l,-1}^{l-1,l-1}$  and  $b = [3(2l+1)/4\pi(2l+3)]^{1/2} C_{l,1,0,0}^{l+1,0} C_{l,1,l,-1}^{l+1,l-1}$  are constants. The Clebsch-Gordon coefficients  $C_{l_1,l_2,m_1,m_2}^{l_f,m_f}$  are used to express constants  $a$  and  $b$ . To obtain the above equation, hydrogen ground state wave function is written as a product of the radial wave function and the spherical harmonic  $Y_{l_i}^{m_i}$ , whereas the wave function for the continuum state is expanded in terms of the spherical Bessel function of first kind  $j_{l_f}$  and the spherical harmonics. The radial transition amplitude is  $d_k^l = \int_0^\infty dr r^{l+3} j_{l_f}(kr) R_{n_i,l_i}(r)$  where  $R_{n_i,l_i}$  is the radial ground-state wave function. Eq. (2) is obtained for twisted XUV pulse, which is linearly polarised along  $x$ -axis and propagating along  $z$ -axis. The form of the vector potential for the Laguerre-Gaussian pulse is taken from Ref. [35, 36].

Due to non-zero OAM of the twisted XUV pulse, three ionising paths are allowed from the unpolarised ground state of hydrogen as evident from Eq. (2). The strength of these paths depend on the magnitudes of  $d_k^l$ ,  $Y_l^n$  and the constants. Possibility of more than one ionising path is a consequence of the modified selection rules. As evident from Eq. (2), the three paths have different contributions from the spherical harmonics  $Y_l^n$ , which depends on the OAM values and determine the resultant angular distribution of the photoelectrons. Let us analyse how

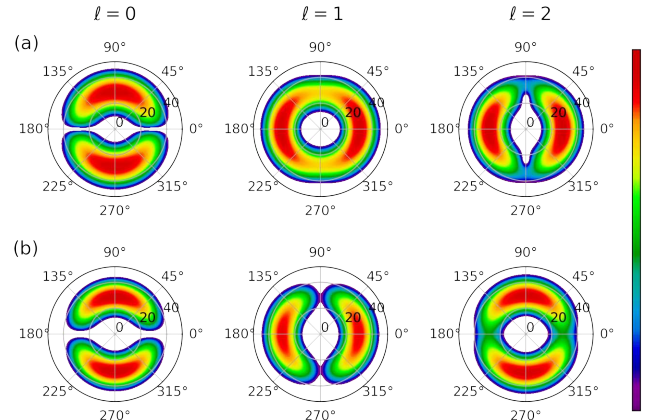


FIG. 1: Normalised photoelectron spectra, induced by twisted XUV pulse, for hydrogen. The spectra are shown as a function of the observational azimuthal angle  $\phi_k$ , the kinetic energy of photoelectron  $E_k$  (shown radially, in eV) and the OAM values of the ionising twisted pulse with Gaussian envelop of 150 attoseconds pulse duration and 46.6 eV photon energy. The spectra are shown for the observational polar angle (a)  $\theta_k = 30^\circ$  and (b)  $\theta_k = 90^\circ$  (shown row-wise).

the photoelectron spectra are sensitive to the OAM of the ionising XUV pulse.

The photoionisation (or unstreaked) spectra, induced by twisted pulse, for different values of the OAM are presented in Fig. 1. The spectra are shown as a function of the observation azimuthal angle  $\phi_k$  and the kinetic energy of the photoelectron  $E_k$  (shown radially in eV). The spectra for two observational polar angles  $\theta_k = 30^\circ$  and  $\theta_k = 90^\circ$  are shown in Figs. 1(a) and 1(b), respectively. The first and third ionisation paths contribute for  $l = 0$  and their photoelectron distributions are given by  $Y_1^1$  and  $Y_1^{-1}$ , respectively [see Eq. (2)]. The nodes in the angular distribution along  $x$ -axis at  $\phi_k = 0^\circ$  and  $\phi_k = 180^\circ$  [see Fig. 2(a) for  $l = 0$ ] are generated due to the fact that the mentioned paths contain equal and opposite real contributions [see Fig. 2(a)]. In contrast to this, the second ionisation path is non-zero for  $l = 1$ , but contributes a constant background to the total spectra as  $Y_0^0$  is angular isotropic. The other two contributing

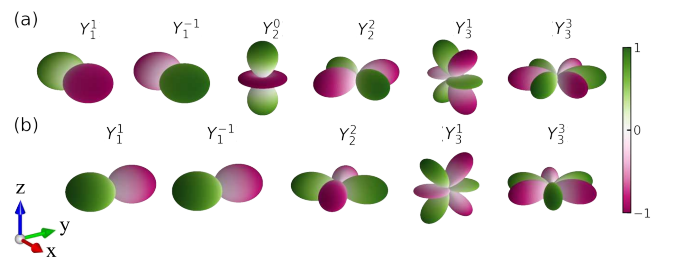


FIG. 2: Normalised (a) real and (b) imaginary parts of the relevant spherical harmonics. The spherical harmonic  $Y_2^0$  is real and  $\text{Im}(Y_2^0)$  is not shown.

terms,  $Y_2^2$  and  $Y_2^0$  (Fig. 2), interfere destructively due to the pre-factors resulting in minimum intensities of the photoelectron distribution along  $y$ -axis, i.e., at  $\phi_k = 90^\circ$  and  $\phi_k = 270^\circ$ . The qualitative behavior of the photo-electron angular distributions for different values of  $\theta_k$  is similar for  $l = 0$  and 1 as visible from Fig. 1.

In case of the twisted pulse with  $l = 2$ , all the three ionisation paths contribute differently for smaller and higher values of  $\theta_k$ . The reason lies in the  $\theta_k$ -dependent distributions of the relevant spherical harmonics, specifically  $Y_3^1$ . The first, second and third ionisation paths correspond to  $Y_3^3$ ,  $Y_1^1$  and  $Y_3^1$ , respectively. The real parts of  $Y_3^3$  and  $Y_3^1$  interfere destructively along  $x$ -axis whereas their imaginary parts interfere constructively along  $y$ -axis for  $\theta_k = 30^\circ$ . Also,  $Y_1^1$  contributes only along  $x$ -axis and results in a maxima along this direction. Thus, in this case, the angular distribution is dominated by the real and imaginary parts of  $Y_3^3$ . However, both the real as well as the imaginary parts of  $Y_3^3$  and  $Y_3^1$  interfere destructively when  $\theta_k$  is close to  $90^\circ$  (see Fig. 2). Therefore, the minima in the angular distribution along  $y$ -axis disappears and appears along  $x$ -axis as  $\theta_k$  increases from smaller to larger values.

From the discussion of Eq. (2) and analysis of Fig. 1, it is established that the unstreaked photoelectron spectra are sensitive to the OAM value of the linearly-polarised ionising pulse. It appears that the presence of the OAM in the ionising pulse can be determined by locating the intensity minima in the unstreaked spectra for smaller values of  $\theta_k$  (say  $\theta_k = 30^\circ$ ). However, the amount of the OAM can not be extracted because of the similar qualitative behavior of the unstreaked spectra for  $l = 1$  and  $l = 2$  [Fig. 1(a)]. Additionally, the unstreaked spectra are not helpful in even determining the presence of the OAM for higher values of  $\theta_k$  [Fig. 1(b)]. Moreover, if circularly polarised twisted XUV pulse is used to ionise the atom, the resultant photoelectron angular distributions are isotropic irrespective of the helicity of the ionising XUV pulse. The spectra are similar for different OAM values as well (not shown here). Thus, it can be concluded that the unstreaked spectra can only determine the presence or absence of the OAM in the ionising pulse, but with many restrictions on the properties of the pulse and the experimental observational setup.

To characterise the exact amount of the OAM encoded in the twisted pulse, it is important to introduce IR pulse to streak the liberated photoelectron. As the unstreaked spectra are sensitive to the observational angle, it is meaningful to use circularly polarised IR pulse, which is represented as

$$\mathbf{E}_L(t) = \frac{\mathcal{E}_L(t)}{\sqrt{2}} [\cos(\omega_L t)\hat{x} - \Lambda_L \sin(\omega_L t)\hat{y}], \quad (3)$$

where  $\mathcal{E}_L(t)$  and  $\Lambda_L$  are the envelop and helicity of the IR pulse, respectively. In this case, the Volkov phase reads

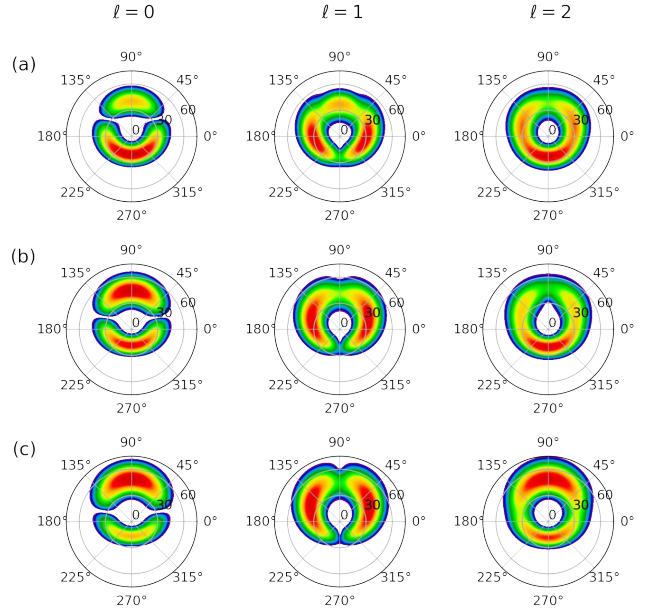


FIG. 3: AAS spectra for different OAM values. The twisted XUV pulse with linear polarisation is used to trigger photoionisation and right-handed circularly polarised IR pulse is used to streak the liberated photoelectrons. The spectra are plotted as functions of  $\phi_k$ ,  $E_k$  (shown radially, in eV) and for (a)  $\theta_k = 30^\circ$ , (b)  $\theta_k = 45^\circ$  and (c)  $\theta_k = 60^\circ$ . All the spectra are normalised with respect to their respective maxima.

as

$$\Phi(\mathbf{k}, t) = -[k^2 + \mathcal{A}_L^2(t)] \frac{t}{2} + \frac{k\mathcal{A}_L(t)}{\omega_L} \sin \theta_k \cos(\omega_L t + \Lambda_L \phi_k). \quad (4)$$

In the following, right-handed circularly polarised IR pulse with 800 nm wavelength is used to streak the photoelectrons. The pulse duration and intensity of the IR pulse are 5 femtoseconds with Gaussian envelope and  $5 \times 10^{13}$  W/cm<sup>2</sup>, respectively. To get the streaking spectra,  $\mathbf{d}_k$  is replaced by  $\mathbf{d}_{p(t)}$ .

AAS spectra for different OAM values are presented in Fig. 3. The vector potential of the streaking IR pulse is directed along negative  $y$ -axis at the instant of ionisation when the time-delay between the twisted XUV and IR pulses is zero. This streaking field induces a change in momentum of the photoelectron  $\delta\mathbf{k} = -\mathbf{A}_L(t)$  [3]. It results in the streaking of the photoelectrons along  $+y$ -direction, i.e.,  $\phi_k = 90^\circ$ . At a first glance, it is evident that the streaking spectra are sensitive to the OAM values as well as to the observation direction of the photoelectrons. On a close inspection of the streaking spectra when  $\theta_k = 30^\circ$ , it is clearly visible that the low-energy regime of the spectra around  $\phi_k = 270^\circ$  are most intense for  $l = 0$  and 2, whereas it is least intense around this region for  $l = 1$  (Fig. 3). Moreover, the numbers of intensity minima in the spectra are 2 for  $l = 0$ , and 3 for  $l = 1$  and  $l = 2$ ; and the angular positions of these minima are different in different spectra. Similar observations can be

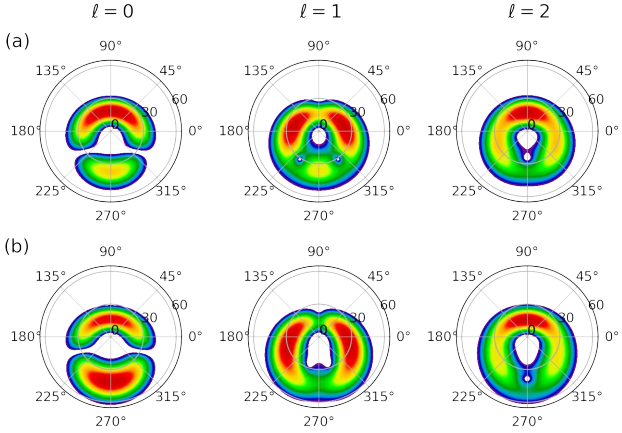


FIG. 4: Same as Fig. 3 except the liberated photoelectrons are streaked by the left-handed circularly polarised IR pulse. The spectra correspond to (a)  $\theta_k = 30^\circ$  and (b)  $\theta_k = 45^\circ$ .

made for  $\theta_k = 45^\circ$  and  $60^\circ$  [Fig. 3(b, c)].

The presence of the three intensity maxima (and lobes) in the spectra for  $l = 1$  at  $\theta_k = 30^\circ$  could be understood as: The streaked part of  $\text{Re}(Y_2^2)$  did not cancel completely by the contribution of  $\text{Re}(Y_2^0)$ ; and  $\text{Im}(Y_2^2)$  contributes in the diagonal directions with respect to the cartesian axes whereas  $\text{Im}(Y_2^0)$  is zero. For  $l = 2$ , the presence of the maxima and minima in intensity at  $\theta_k = 30^\circ$  is decided dominantly by the first ionisation path, which is governed by  $Y_3^3$ . As the value of  $\theta_k$  increases, other ionisation paths ( $Y_2^2$  for  $l = 1$ ;  $Y_1^1$  and  $Y_3^1$  for  $l = 2$ ) contribute significantly, which results in the suppression of one of the three lobes and decides the angular modulation of the streaking spectra [middle and right columns in Fig. 3]. For  $l = 2$ , a major distinction in the streaking spectra is observed at  $\theta_k = 60^\circ$ . The reason lies in the angular structure of  $Y_3^1$ , which governs the third ionisation path. For different values of  $\theta_k$ , different lobes of  $Y_3^1$  contribute with a threshold at approximately  $\theta_k = 50^\circ$ , i.e., the contribution of  $Y_3^1$  reverses when  $\theta_k$  crosses  $50^\circ$ . Thus giving similar spectra for  $\theta_k = 30^\circ$  and  $\theta_k = 45^\circ$ ; and for  $\theta_k = 60^\circ$  and  $\theta_k = 90^\circ$  (not shown here). The distinction and uniqueness of the streaking spectra, i.e., the angular modulation (maxima and minima) in the intensity profile along with the strength of the minima, prove useful to discern the units of OAM encoded in the twisted pulse.

Furthermore, instead of right-handed circularly polarised IR pulse, left-handed circularly polarised IR pulse is used for streaking to explore any possibility of the circular dichroism. Figure 4 presents the streaking spectra corresponding to left-handed circularly polarised IR streaking pulse for  $\theta_k = 30^\circ$  and  $45^\circ$ . In this case, the vector potential of the IR pulse is along  $+y$  direction, which results in streaking of photoelectrons along  $-y$  direction. Therefore, all the spectra are streaked along the negative direction in comparison to the case when right-

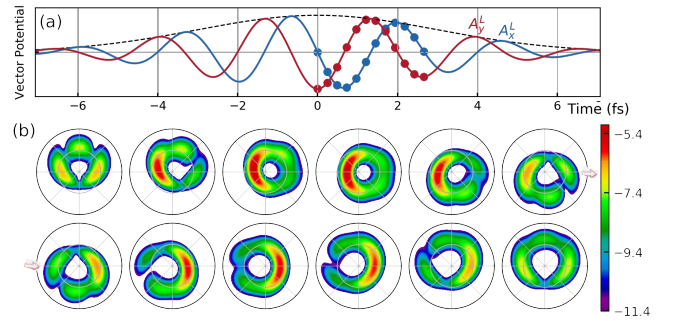


FIG. 5: (a) Vector potential of the right-handed circularly polarised IR streaking pulse. The  $x$ - and  $y$ -components are shown in blue and red colours, respectively. (b) For  $l = 1$ , the attosecond streaking spectra observed at  $\theta_k = 30^\circ$  corresponding to the various time-delays between the IR and twisted pulse. The twisted pulse is delayed in steps of 10 a.u. for one complete cycle of the IR pulse (2.67 fs or 110 a.u.).

handed circularly polarised IR pulse is used to streak the photoelectrons. It is established from Figs. 3 and 4 that the streaking spectra are distinct and unique for each values of the OAM encoded in the twisted pulse.

Till now we have discussed AAS when the time-delay between both the pulses is zero. To explore how the streaking spectrum changes as the time-delay between both the pulses is varied, several streaking spectra, along with the  $x$ - and  $y$ -components of the right-handed IR pulse, for  $l = 1$  at  $\theta_k = 30^\circ$  is presented in Fig. 5. The twisted pulse is delayed in steps of 10 a.u. for a complete cycle of the IR pulse. As the time-delay is increased, the vector potential of the IR pulse rotates clockwise starting from  $-y$  direction. So, the photoelectrons are streaked along  $+y$  direction initially and later follows the  $\mathbf{A}_L(t)$  accordingly. Also, the intensity of the spectra follow the envelope of the IR pulse. It is evident from the streaking spectra that the number of lobes are preserved as the time-delay is varied.

In conclusion, we can summarise that the AAS spectra encode the signature and the amount of the OAM present in the twisted attosecond pulse. As a result in the modifications of the selection rules, several ionising paths by twisted pulse are possible, which results in angular modulations of the photoelectron spectra. By choosing specific observation directions of the photoelectrons, AAS technique is useful for linear, right as well as left circular polarisations of the unknown pulse. We believe that our proposed approach will be the core ingredient in the light-matter interaction induced by twisted attosecond pulses. The present work paves the route to study helical light-matter interaction and twisted pulse mediated strong-field ionization via streak camera [37].

G. D. acknowledges support from Science and Engineering Research Board (SERB) India (Project No. ECR/2017/001460) and Max-Planck India visiting fellowship.

\* gdixit@phy.iitb.ac.in

- 
- [1] F. Krausz and M. I. Stockman, *Nature Photonics* **8**, 205 (2014).
- [2] F. Krausz and M. Ivanov, *Reviews of Modern Physics* **81**, 163 (2009).
- [3] J. Itatani, F. Quéré, G. L. Yudin, M. Y. Ivanov, F. Krausz, and P. B. Corkum, *Physical Review Letters* **88**, 173903 (2002).
- [4] M. Kitzler, N. Milosevic, A. Scrinzi, F. Krausz, and T. Brabec, *Physical Review Letters* **88**, 173904 (2002).
- [5] P. M. Paul, E. S. Toma, P. Breger, G. Mullot, F. Augé, P. Balcou, H. G. Muller, and P. Agostini, *Science* **292**, 1689 (2001).
- [6] Y. Mairesse and F. Quéré, *Physical Review A* **71**, 011401 (2005).
- [7] F. Quéré, Y. Mairesse, and J. Itatani, *Journal of Modern Optics* **52**, 339 (2005).
- [8] P. L. He, C. Ruiz, and F. He, *Physical Review Letters* **116**, 203601 (2016).
- [9] Á. Jiménez-Galán, G. Dixit, S. Patchkovskii, O. Smirnova, F. Morales, and M. Ivanov, *Nature Communications* **9**, 1 (2018).
- [10] L. Allen, M. W. Beijersbergen, R. J. C. Spreeuw, and J. P. Woerdman, *Physical Review A* **45**, 8185 (1992).
- [11] F. Cardano and L. Marrucci, *Nature Photonics* **9**, 776 (2015).
- [12] M. Babiker, D. L. Andrews, and V. E. Lembessis, *Journal of Optics* **21**, 013001 (2018).
- [13] S. Fürhapter, A. Jesacher, S. Bernet, and M. Ritsch-Marte, *Optics Express* **13**, 689 (2005).
- [14] K. A. Forbes, *Phys. Rev. Letts.* **122**, 103201 (2019).
- [15] W. Brullot, M. K. Vanbel, T. Swusten, and T. Verbiest, *Science advances* **2**, e1501349 (2016).
- [16] K. A. Forbes and D. L. Andrews, *Optics Letters* **43**, 435 (2018).
- [17] M. F. Andersen, C. Ryu, P. Cladé, V. Natarajan, A. Vaziri, K. Helmerson, and W. D. Phillips, *Physical Review Letters* **97**, 170406 (2006).
- [18] R. Inoue, N. Kanai, T. Yonehara, Y. Miyamoto, M. Koashi, and M. Kozuma, *Physical Review A* **74**, 053809 (2006).
- [19] T. Ruchon and M. Fanciulli, arXiv preprint arXiv:2005.08349 (2020).
- [20] M. Zürch, C. Kern, P. Hansinger, A. Dreischuh, and C. Spielmann, *Nature Physics* **8**, 743 (2012).
- [21] C. Hernández-García, A. Picón, J. San Román, and L. Plaja, *Physical Review Letters* **111**, 083602 (2013).
- [22] G. Gariepy, J. Leach, K. T. Kim, T. J. Hammond, E. Frumker, R. W. Boyd, and P. B. Corkum, *Physical Review Letters* **113**, 153901 (2014).
- [23] R. Géneaux, A. Camper, T. Auguste, O. Gobert, J. Caillet, R. Taïeb, and T. Ruchon, *Nature Communications* **7**, 12583 (2016).
- [24] L. Rego, J. San Román, A. Picón, L. Plaja, and C. Hernández-García, *Physical Review Letters* **117**, 163202 (2016).
- [25] A. Turpin, L. Rego, A. Picón, J. San Román, and C. Hernández-García, *Scientific Reports* **7**, 43888 (2017).
- [26] C. Hernández-García, A. Turpin, J. San Román, A. Picón, R. Drevinskas, A. Cerkauskaitė, P. G. Kazansky, C. G. Durfee, and Í. J. Sola, *Optica* **4**, 520 (2017).
- [27] W. Paufler, B. Böning, and S. Fritzsche, *Physical Review A* **98**, 011401 (2018).
- [28] D. Gauthier, S. Kaassamani, D. Franz, R. Nicolas, J. T. Gomes, L. Lavoute, D. Gaponov, S. Février, G. Jargot, M. Hanna, et al., *Optics Letters* **44**, 546 (2019).
- [29] D. Gauthier, P. R. Ribić, G. Adhikary, A. Camper, C. Chappuis, R. Cucini, L. F. DiMauro, G. Dovillaire, F. Frassetto, R. Géneaux, et al., *Nature Communications* **8**, 14971 (2017).
- [30] F. Kong, C. Zhang, F. Bouchard, Z. Li, G. G. Brown, D. H. Ko, T. J. Hammond, L. Arissian, R. W. Boyd, E. Karimi, et al., *Nature Communications* **8**, 14970 (2017).
- [31] K. M. Dorney, L. Rego, N. J. Brooks, J. San Román, C. T. Liao, J. L. Ellis, D. Zusin, C. Gentry, Q. L. Nguyen, J. M. Shaw, et al., *Nature Photonics* **13**, 123 (2019).
- [32] T. Kaneyasu, Y. Hikosaka, M. Fujimoto, T. Konomi, M. Katoh, H. Iwayama, and E. Shigemasa, *Physical Review A* **95**, 023413 (2017).
- [33] B. Böning, W. Paufler, and S. Fritzsche, *Physical Review A* **96**, 043423 (2017).
- [34] S. Giri, M. Ivanov, and G. Dixit, *Physical Review A* **101**, 033412 (2020).
- [35] A. Picón, A. Benseñy, J. Mompart, J. R. V. de Aldana, L. Plaja, G. F. Calvo, and L. Roso, *New Journal of Physics* **12**, 083053 (2010).
- [36] A. Picón, J. Mompart, J. R. V. de Aldana, L. Plaja, G. F. Calvo, and L. Roso, *Optics Express* **18**, 3660 (2010).
- [37] M. Kübel, Z. Dube, A. Y. Naumov, M. Spanner, G. G. Paulus, M. F. Kling, D. M. Villeneuve, P. B. Corkum, and A. Staudte, *Physical Review Letters* **119**, 183201 (2017).